Nanoscale Res Lett (2010) 5:195–204
DOI 10.1007/s11671-009-9465-9

NANO EXPRESS

Alternating Magnetic Field Controlled, Multifunctional Nano-Reservoirs: Intracellular Uptake and Improved Biocompatibility

Santaneel Ghosh · Somesree GhoshMitra · Tong Cai · David R. Diercks · Nathaniel C. Mills · DiAnna L. Hynds

Received: 7 September 2009 / Accepted: 5 October 2009 / Published online: 25 October 2009

Abstract Biocompatible magnetic nanoparticles hold great therapeutic potential, but conventional particles can be toxic. Here, we report the synthesis and alternating magnetic field dependent actuation of a remotely controllable, multifunctional nano-scale system and its marked biocompatibility with mammalian cells. Monodisperse, magnetic nanospheres based on thermo-sensitive polymer network poly(ethylene glycol) ethyl ether methacrylate-*co*-poly(ethylene glycol) methyl ether methacrylate were synthesized using free radical polymerization. Synthesized nanospheres have oscillating magnetic field induced thermo-reversible behavior; exhibiting desirable characteristics comparable to the widely used poly-*N*-isopropylacrylamide-based systems in shrinkage plus a broader volumetric transition range. Remote heating and model drug release were characterized for different field strengths. Nanospheres containing nanoparticles up to an iron concentration of 6 mM were readily taken up by neuron-like PC12 pheochromocytoma cells and had reduced toxicity compared to other surface modified magnetic nanocarriers. Furthermore, nanosphere exposure did not inhibit the extension of cellular processes (neurite outgrowth) even at high iron concentrations (6 mM), indicating minimal negative effects in cellular systems. Excellent intracellular uptake and enhanced biocompatibility coupled with the lack of deleterious effects on neurite outgrowth and prior Food and Drug Administration (FDA) approval of PEG-based carriers suggest increased therapeutic potential of this system for manipulating axon regeneration following nervous system injury.

Keywords Magnetic actuation · Biomaterials · Thermo-sensitive polymers · Nano-biotechnology · Biocompatibility · Neuron

S. Ghosh (✉)
Department of Physics and Engineering Physics, Southeast Missouri State University, MS 6600, One University Plaza, Cape Girardeau, MO 63701, USA
e-mail: sghosh@semo.edu

S. GhoshMitra · N. C. Mills · D. L. Hynds
Department of Biology, Texas Woman's University, PO Box 425799, Denton, TX 76204, USA

T. Cai
Department of Physics, University of North Texas, Denton, TX 76203, USA

D. R. Diercks
Center of Advancement of Research and Technology, University of North Texas, Denton, TX 76207, USA

Introduction

Treatment potential for many biomedical conditions is limited by the lack of therapeutics that can be efficiently targeted and precisely controlled. For instance, functional recovery following neurotraumatic injury could be facilitated by therapeutics for guided axon regeneration [1]. Axon growth can be directed by magnetic or electrical fields alone [2–4], but a more manipulable system that provides precisely tunable therapeutic delivery may offer enhanced potential to direct axon regeneration and guidance to targets. Nano-structured materials and smart surfaces provide great potential for developing such novel biomedical therapeutics [5–8]. However, several issues limit the use of conventional magnetic nanoparticles for biomedical applications. Magnetic nanoparticles alone are highly toxic, but excipients can facilitate their delivery to cells [9]. Several groups have synthesized magnetic

nanoparticle systems using smart polymers like poly (*N*-isopropylacrylamide) (PNIPAM) [10–12]. However, PNIPAM based systems have low biocompatibility because the NIPAM monomer is carcinogenic and teratogenic [13]. Dimercaptosuccinic acid (DMSA) coated particles enhances intracellular uptake, but the surface functionalization does not improve the biocompatibility of the nanomagnets [14]. Traditional polyethylene glycol (PEG) coating reduces toxicity, but it does not retain thermo-sensitive behavior or external tunability. Thus, development of a highly biocompatible, non-toxic and highly tunable nanoparticle system is necessary. Ideally, the constructed materials should: (1) minimize toxicity, (2) control intracellular functions like temperature or pH, and (3) elicit a fast response to external stimuli (e.g., ac magnetic field). A system that meets these goals possesses enhanced potential for combinatorial therapeutics. For example, simultaneous use of hyperthermia and low doses of chemotherapeutic agents decreases tumor growth by targeted cytotoxicity with reduced systemic effects [15].

For axon regeneration, a system that allows manipulation of cellular function or delivery of drugs through regulation of temperature and/or magnetic fields may be ideal. PNIPAM coated nanomagnets are attractive because of their perceived intelligence to external stimuli. For instance, they have a lower critical solution temperature (LCST) close to the normal physiological temperature (~33 °C), allowing size tunability and therefore controlled release of small molecules around 33–35 °C [16]. However, it is necessary to tune the LCST in the range of 33–42 °C for certain biomedical applications requiring volumetric transition at higher temperatures. Recently, LCSTs of polyethylene glycol (PEG) based systems have been tailored between 24 and 42 °C by changing the molar ratio and molecular weight of the copolymers [17, 18]. It is also possible to regulate pressure/flow/temperature in micrometer or sub-micrometer range by using tunable magnetic nanocrystals embedded in thermo-sensitive polymer networks [19]. Since PEG is non-toxic, anti-immunogenic and approved by the FDA [9, 17], the potential of magnetic modulation makes it an attractive alternative for overcoming traditional difficulties in actuating conventional micro- or nano-structures using chemical, mechanical or thermal excitation [20–22]. Although optical actuation may be used, its application for use in vivo is limited. Moreover, magnetic actuation could use remotely applied ac and dc fields to regulate intracellular temperature [23], control the release of drug from the tunable excipient by regulating swelling/shrinkage behavior [12] and manipulate cellular functions (e.g., axon growth) within tissues [17]. Thus, using tunable PEG derivatives to encapsulate nanomagnets may facilitate the simultaneous regulation of localized temperature and sustained release of pharmaceuticals to the targeted cells in clinical practice.

In this study, we report synthesis and actuation of low toxicity magnetic nanospheres and assessed their effect on PC12 cell viability and morphology. Copolymers of 2-(2-methoxyethoxy)ethyl methacrylate and oligo(ethylene glycol) methacrylate ($PEGETH_2MA$-*co*-PEGMA) based hydrogels were synthesized to encapsulate ferromagnetic nano-particles. The polymeric shell acts as the reservoir of the drug molecules, while the magnetic core acts as nano-source of heat when exposed to the ac magnetic field. To our knowledge, this is the first time that ac field modulated remote actuation, model drug release and cytotoxicity is assessed for monodisperse, novel nanospheres that are made of all biocompatible and tunable polymers.

Experimental Techniques

Nanosphere Synthesis

We synthesized ferromagnetic nanoparticles (Fe_3O_4) encapsulated within the thermo-activated polymer network of $PEGETH_2MA$-*co*-PEGMA using free radical polymerization (Scheme 1). In 200 mL of deionized (DI) water were dissolved 6.4 g of $PEGETH_2MA$ ($M_n \sim 246$ g mol^{-1}, Aldrich), 1.57 g PEGMA ($M_n \sim 300$ g mol^{-1}, Aldrich), 0.12 g Fe_3O_4, 0.064 g sodium dodecyl sulfate (SDS) and $4.6'10^{-4}$ mol of ethylene glycol dimethacrylate (EGDMA 97%, Fluka). The solution was purged with nitrogen gas for 40 min at 70 °C. Ammonium persulfate (APS, 0.20 g), which was dissolved in 5 mL of water, was then added to initiate the emulsion copolymerization. The reaction lasted for 12 h under nitrogen gas bubbling atmosphere. The nanospheres were purified via a dialysis tube (MW cut-off 13, 000) against water for 7 days at room temperature, while the de-ionized water was exchanged twice a day, and collected by ultra centrifugation. Thermogravimetric analysis (TGA) was performed to quantify the polymer and nanomagnet concentration after synthesis. Vitamin B_{12} (MW 1356) was used as model drug for ac field modulated release demonstration. Magnetic nanospheres and the control polymeric nanoparticles (without magnetic core) are used for release experiment. Aqueous solution of vitamin B_{12} (20 mg/mL) was added to the freeze-dried nanospheres. The solution was stirred for 8 h at 25 °C. Drug loaded particles were collected by ultra centrifugation. The release behavior was studied in insulated plastic reaction vessels containing the nanosphere solution. Two separate conditions were maintained: (a) ac field exposure (100 Oe, 150 kHz), and (b) dc field exposure (100 Oe, 0 Hz). The supernatant was collected at every time point following the ac/dc field exposure, and the particles are re-dispersed. Time dependent release was quantified as mass released at time t, M_t, over the total mass released, M_{cum} (96 h) using a

UV–Vis spectrometer. To minimize Joule heating, ac field was switched on for 20 min, following 40 min off cycles. For uptake assessment, fluorescent nanospheres were synthesized by conjugating with methacryloxyethyl thiocarbamoyl rhodamine B fluorescent monomers (Polysciences, Inc., emission: 570 nm) during the copolymerization reaction. Fluorescence intensity is easily varied by adjusting the amount of fluorescent monomer during reaction and in this study, 1 mg of monomer is added per 6 gm of copolymer content. Any unreacted fluorescent monomer was removed by dialysis for 7 days.

Scanning and Transmission Electron Microscopy

Sphere morphology was assessed using an FEI QUANTA 200 scanning electron microscope (SEM). A Philips EM 420 transmission electron microscope (TEM) was used to simultaneously observe polymer encapsulation and the embedded magnetic nanoparticles (core–shell structure). Cryo-immobilization was performed to prevent the nanospheres from collapsing during electron microscopy. Accelerating voltage during SEM imaging was kept between 5 and 20 kV; TEM analysis was performed with 120 kV electron beam.

Light Scattering and Magnetic Measurements

For the dynamic light scattering (DLS) experiment, a laser light scattering spectrometer (ALV, Germany) equipped with an ALV-5000 digital time correlator was used with a helium–neon laser (Uniphase 1145P, wavelength of 632.8 nm) as the light source. The hydrodynamic radius distribution of the nanospheres in water was measured at a scattering angle of 60°. A homemade magnetic field generator was designed to extract the AC field induced heating response. This device consists of an AC signal generator, a power amplifier, and a copper coil (diameter 25 mm, coil quality factor ~70). The coil was an element of a resonant RLC circuit with a self-inductance of 48 μH. The field strength was calculated using a high-frequency current probe (Tektronix) and an oscilloscope (Agilent). Custom software (written in LabView) controls the signal. Magnetic property [$M(H)$] of the nanospheres was measured using a Lakeshore model 7300 vibrating sample magnetometer (VSM) at ambient temperature.

Cell Culture and Treatment

PC12 rat pheochromocytoma cells (ATCC, Manassas, VA) were used to assess nanosphere biocompatibility. Cells were routinely cultured at 37 °C in 5% CO_2 in F-12 nutrient mixture with Kaighn's modification (F12 K) containing 2.5% fetal bovine serum and 15% horse serum (both from Invitrogen, Carlsbad, CA). For experiments, cells were plated at 10,000 cells/cm^2 on glass coverslips in 24-well tissue culture plates and allowed to grow for 48 h. Cultures were washed twice with phosphate buffered saline (PBS) and placed into serum- and phosphate-free HEPES-buffered Dulbecco's modified Eagle's medium (DMEM, Invitrogen, Carlsbad, CA) to prevent particle aggregation. Nanospheres were added at final iron concentrations (assessed by TGA analysis) of 0, 0.34, 3.4, 6.0 or 16 mM for 48 h.

Assessment of Particle Internalization

PC12 cells were exposed for 48 h at 37 °C to fluorescent nanospheres containing magnetic nanoparticles at an iron

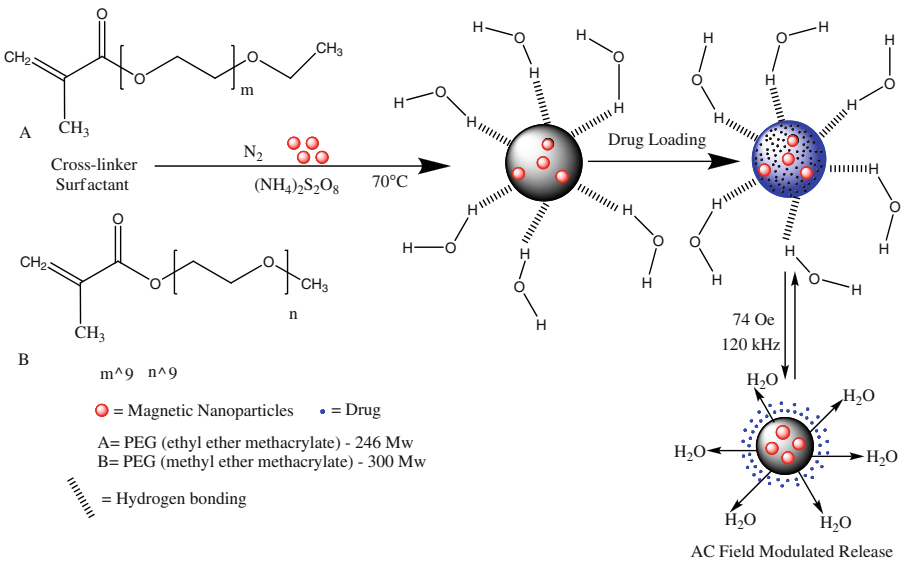

Scheme 1 Synthesis of core–shell nanospheres and oscillating field induced actuation

concentration of 3.4 mM. Cultures were washed with PBS to remove extracellular nanoparticles, and cells were incubated for 24 more hours at 37 °C. Cultures were fixed for 20 min in 4.0% paraformaldehyde and 2.0% glutaraldehyde in PBS at room temperature. Images were captured through a 64× objective in differential interference contrast (DIC) and tetramethylrhodamine isothiocyanate (TRITC, Ex = 568 nm, Em = 585/40 nm) channels using a Zeiss Axiovert 200 M microscope (Zeiss, Thornwood, NJ) fitted with a Yokogawa CSU-10 confocal scanner and a Hamamatsu camera (McBain Instruments, Simi Valley, CA).

Assessment of Cell Viability

After exposure to magnetic nanospheres, cells were washed twice in PBS and viability was assessed using the Live/Dead viability/cytotoxicity assay (Invitrogen, Carlsbad, CA), according to the manufacturer's directions. In brief, cultures were double-labeled with calcein AM, which permeates cell membranes and becomes fluorescent when exposed to esterase activity in living cells, and ethidium homodimer-1 (EthD1), which is excluded by the plasma membrane from living cells but crosses the compromised membrane of damaged cells to bind nucleic acids and fluoresce. Digital images were captured through a 10× objective on a Zeiss Aviovert 200 M microscopy (Zeiss, Thornwood, NJ) in fluorescein isothiocyanate (FITC, Ex = 480/30 nm, Em = 535/40 nm) and TRITC (Ex = 540/25 nm, Em = 605/55 nm) channels for calcein AM and EthD1, respectively. Only non-aggregated single cells (at least 300 cells/condition) were quantified, and the percent of viable cells was calculated. Significant differences between magnetic nanospheres containing different concentrations of iron were determined by ANOVA with subsequent Tukey post-hoc tests. Nuclear morphology was assessed using confocal images captured through a 64× objective from cells labeled with 4′,6-diamidino-2-phenylindole (DAPI, Ex = 405 nm, Em = 450/35 nm), following exposure to nanospheres containing magnetic nanoparticles at different concentrations of iron.

Assessment of Cell Morphology, Cytoskeleton and Neurite Outgrowth

Following nanosphere exposure, cultures were washed twice with PBS and placed into serum-free F-12 K for 72 h with or without 100 ng/mL nerve growth factor β subunit (β-NGF, Sigma–Aldrich, St. Louis, MO) being added daily. Cultures were fixed in 4.0% paraformaldehyde and 2.0% glutaraldehyde in PBS, washed twice in PBS, and blocked for 30 min in PBS containing 1.5% normal donkey serum and 0.1% Triton X-100 at room temperature. Samples were double labeled for filamentous actin and tubulin by sequential exposure to 3.3 μM Texas Red-X phalloidin (30 minutes, Invitrogen, Carlsbad, CA) and rabbit anti-βIII tubulin (1:200, overnight, Abcam, Cambridge MA). Tubulin immunoreactivity was visualized by Alexafluor 488-conjugated donkey anti-rabbit secondary antibodies (1:200, 1 h, Invitrogen, Carlsbad, CA). Digital images were captured though a 40× objective using DIC optics, and through a 64× objective in TRITC (Ex = 568 nm, Em = 585/40 nm) and FITC (Ex = 488 nm, Em = 520/35 nm) channels on a Zeiss Axiovert 200 M microscope with confocal attachments (McBain Instruments, Simi Valley, CA).

Neurite outgrowth was assessed using the percent of neurite-bearing cells, determined from phase contrast images (five images/condition/experiment) captured through a 40× objective on a Zeiss Axiovert 200 M microscope. For this analysis, a neurite was defined as a cellular extension that exceeded 10 μm. Only non-aggregated cells where the cell and all its neurites were included in the image were quantified, and imaged fields were systematically selected from each quadrant and the center of each coverslip to ensure a representative sample. Differences between experimental conditions were determined by ANOVA with subsequent Tukey post-hoc test using a significance level of $\alpha = 0.05$.

Results and Discussion

It was important to design a system where the polymer encapsulates the magnetic nanoparticles to facilitate solubility and bioavailability and also provides the potential to conjugate bioactive peptides, antibodies, oligonucleotides or drugs. Thus, a key feature was to design a PEG-based system with a tunable LCST close to physiological temperature. Based on previous reports [17, 18], we chose a molar ratio of PEGMA to PEGETH$_2$MA of 20%. Unlike single domain crystals, multi-domain magnetic particles exhibit primarily hysteresis loss-induced heating inside the ac field exposure with low frequency. Hysteresis loss induced heating is preferred over relaxation loss because the former is easier to tune by the controlled modulation of the oscillating magnetic field, especially considering the sharp hydrodynamic radius change that may occur around the LCST and severely impact the Brownian relaxation loss. To maximize the energy absorption, nanomagnet size was chosen to be in the range of 25–30 nm, close to the ferromagnetic exchange length (27 nm) for magnetite [24].

Physiochemical Characterization of Magnetic Nanospheres

The nanospheres exhibited good colloidal stability in aqueous solution with no obvious precipitation after

several days. We initially assessed particle size and morphology using SEM. Spherical particles were observed (Fig. 1a), and the mean diameter was found to be 315 ± 23 nm. No magnetic nanoparticles were observed on the surface of the nanospheres, which is an indirect proof of polymer encapsulation. The lower electron beam energy (5–30 kV) of SEM imaging was insufficient to penetrate the outer polymer layer, so we directly assessed particle encapsulation by TEM. At an accelerating voltage of 90 kV, electrons were able to pierce through the outer polymer shell. The resulting TEM micrographs revealed that the nanomagnets were mostly concentrated near the center of the nanospheres (Fig. 1b). The individual particles were located near each other, but they were separated and did not agglomerate. We interpret these results as validation that the synthesis did indeed produce nanospheres with a hydrophobic core that had limited or no particle agglomeration (even at higher concentrations), which would have resulted in subsequent reduction in coercivity.

The temperature dependence of normalized hydrodynamic radii (R_h) of the magnetic nanospheres was probed by performing the DLS measurement (Fig. 2). Here, the radii [$R_h(T)$] are divided by the value at 22 °C [$R_h(22)$], and the molecular weight of PEGMA is fixed at 300 Da. The volumetric transition occurred between 31 and 41 °C and included a sharper change or LCST at around 36 °C. The broader transition range was attributed to the free radical polymerization process, where polymer chains are initiated all along the reaction, and therefore strong chain-to-chain deviations of composition can be expected. This transition range is broader than that of the PNIPAM nanospheres, which have homogeneous composition and therefore, a sharp transition [25]. Volumetric change is seen to be unaffected due to nanomagnet doping compared to the non-magnetic PEG nanospheres having similar compositions, justifying the use of optimal concentration of magnetic particles. LCST of the nanospheres can be elevated/lowered to a desired temperature based on PEGMA molecular weight and molar ratio and currently being investigated. Magnetic properties of the doped PEGETH$_2$MA-*co*-PEGMA nanosphere aqueous dispersion (10 wt% polymer concentration; i.e., 3.5 mg/mL Fe_3O_4, determined by TGA analysis) were probed by performing the VSM measurements (Fig. 2, *Inset*). The hysteresis response reveals the ferromagnetic characteristics of the nanospheres. From the TEM micrographs, we observed that the nanomagnets did not agglomerate after repeated heating cycles, possibly because of the lower residual magnetism (0.314×10^{-2} emu/gm) of the particles.

Response to Alternating Magnetic Field and Drug Release

We next measured the remote heating response of the nanospheres in an ac magnetic field (125 Oe, 120 kHz). Temperature inside the insulated plastic reaction vessels containing the nanosphere solutions was monitored by a fiber optic temperature sensor (Photon Control Inc.,). Copolymer concentrations were varied from 10 to 0.1 wt%, resulting in nanomagnet concentration of 3.5 to 0.035 mg/mL (∼45–0.45 mM Fe). Upon application of the field, the measured temperature of the nanosphere solutions increased in a concentration-dependent manner and reached a near steady state after ∼30 min (Fig. 3a). For any specific concentration of nanomagnets, similar temperature regulation capability is achieved as a function of ac field intensity. As speculated from the minor hysteresis loops, the effective heating is observed only above a threshold field (∼37 Oe, not shown here). Finally, ac field dependent release of vitamin B_{12} is demonstrated in Fig. 3b. Oscillating field induced heating and subsequent shrinkage of the hydrogel network led to enhanced release of the loaded drug from the magnetic nanospheres. However, ac field was unable to heat the control nanospheres and did not cause accelerated release from them. Moreover, it is also observed that the applied dc field had minimal effect on the release profile for both magnetic and the

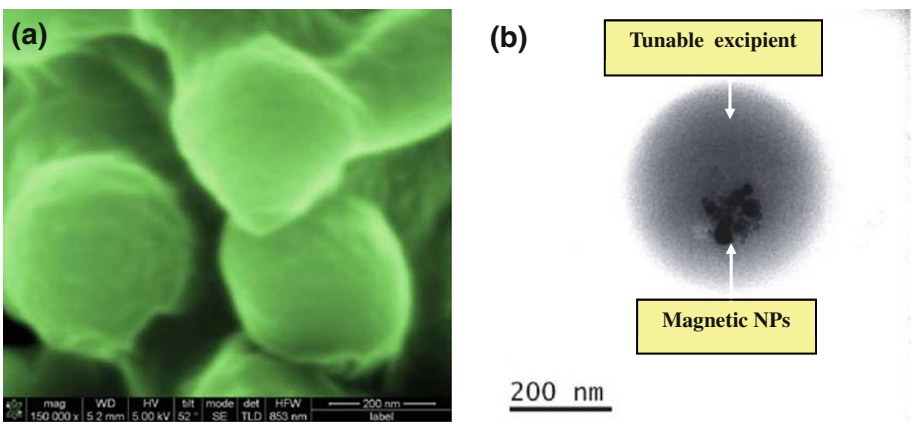

Fig. 1 **a** SEM, and **b** TEM micrographs of the magnetic nanospheres; nanomagnets are not visible through the polymer layer in SEM images, while the TEM micrograph (90 kV) captures the polymer encapsulation and the embedded nanoparticles simultaneously

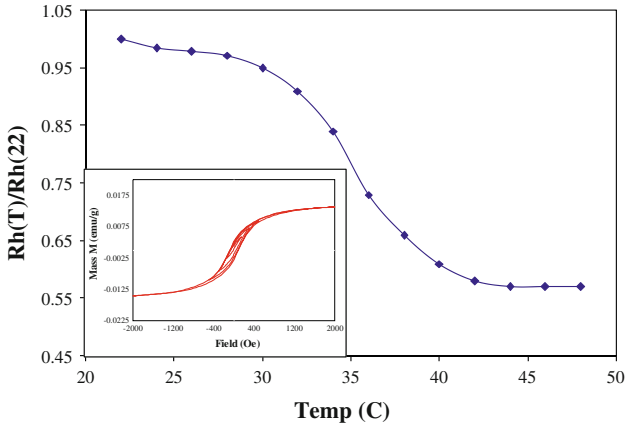

Fig. 2 Thermo-responsive behavior of magnetic nanospheres from DLS measurement. $R_h(T)$ represents the hydrodynamic radius at any temperature T, and $R_h(22)$ represents the radius at 22 °C. *Inset*: Minor hysteresis loop amplitudes of the nanospheres, revealing loop area dependence (equivalent to power loss) with increasing field intensity

control particles. As the nanosphere temperature can be tailored by controlled modulation of field intensity and nanomagnet loading, we interpret these results to indicate that the system may be precisely manipulated using external ac magnetic fields to alter the release profile or sequential release.

Magnetic Nanosphere Internalization into Neuron-Like Cells

To affect cellular functions, magnetic nanospheres must gain entry into cells. We assessed cellular uptake using fluorescent magnetic nanospheres and confocal microscopy. Cells not exposed to nanospheres displayed morphology typical of PC12 cells (Fig. 4a) and had minimal fluorescence in confocal sections taken through the center of each cell (Fig. 4b). In comparison, exposure to magnetic nanospheres did not alter cell morphology (Fig. 4c). Similar to previous results [26–28], fluorescent nanospheres were readily internalized (Fig. 4d). Interestingly, the pattern of internalization in the current study was more indicative of a cytosolic distribution, compared to the typical punctuate endosome distribution seen in the earlier reports. It is possible that 48 h of exposure to magnetic nanospheres allowed translocation of the nanospheres from endocytotic vesicles to the cytosol. However, endocytotic distribution was still observed in non-neuronal cells 3 days after nanoparticle exposure [28], perhaps reflecting a cell type-specific response. In this analysis, we observed that nearly 100% of the cells internalized magnetic nanospheres within 48 h. That the synthesized nanospheres are so readily internalized has important implications for the potential of this system to be useful in biomedical therapeutics. In addition, these results also indicate the ease of

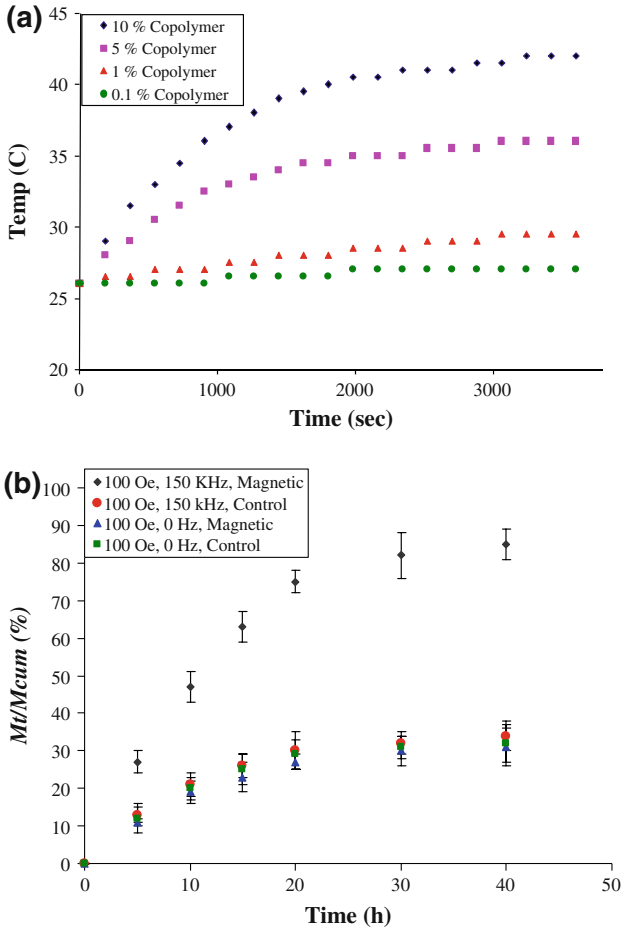

Fig. 3 **a** Hysteresis induced heating of magnetic nanosphere solutions. Polymer content was varied from 10 to 0.1 wt%, resulting in nanomagnet concentration from 3.5 to 0.035 mg/mL, respectively. Measured with oscillating field strength of 125 Oe and a frequency of 120 kHz, sample volume was 5 mL. **b** AC field modulated vitamin B_{12} release from the magnetic nanospheres. M_t represents mass released at any time t, and M_{cum} represents total mass released over 96 h

derivatizing the polymer shell, potentially providing an efficient method to target the nanosphere to particular cells. For instance, by selecting a proper initiator and surfactant, it is possible to synthesize nanospheres with amino or carboxyl functional groups to allow covalent attachment of peptides at either the carboxy or amino termini. Targeted delivery could be achieved by attaching a peptide ligand for a neuron-specific receptor (e.g., attaching the β subunit of nerve growth factor for targeting trkA expressing neurons), similar to strategies previously reporting for targeting nanoparticle systems to particular cell types [29–31]. In addition, this could allow measured release of incorporated drugs or peptides using oscillating magnetic fields, creating highly diverse therapeutic potential for the synthesized system [27, 32].

Magnetic Nanospheres are Minimally Toxic to Neuron-Like Cells

To be useful in biomedical applications, the constructed nanospheres must have low toxicity and little innate bioreactivity. We assessed the cytotoxicity of the magnetic nanospheres using a Live/Dead assay. In this assessment, living cells incorporated calcein AM and remained impermeable to ethidium homodimer 1 (EthD1), thereby exhibiting green fluorescence. Dead or dying cells allowed EthD1 to cross their compromised membranes and exhibited red fluorescence. Fluorescent images of PC12 cells not exposed to magnetic nanospheres had a very low basal level of cell death (Fig. 5a). Comparable levels of cell death were seen in cells exposed for 48 h to nanospheres containing magnetic nanoparticles corresponding to 3.4 mM iron (Fig. 5b). For nanospheres containing higher levels of magnetic nanoparticles (e.g., an iron concentration of 16 mM), toxicity increased (Fig. 5c). Quantification (Fig. 5d) indicated a significant effect of magnetic nanoparticle concentration on cell viability ($F_{3,11} = 22.741$, $p = 0.001$), but confirmed there was no difference between cells exposed to nanospheres with iron concentrations up to 3.4 mM ($p > 0.98$). However, cell viability was decreased by nanospheres containing magnetic nanoparticles with 16 mM iron concentration ($p = 0.001$). Based on prior work using magnetic nanoparticles, we assume that cell death occurred through an apoptotic mechanism. We did not completely analyze this, but did assess nuclear morphology and found little fragmentation and blebbing or DNA condensation in cells not exposed to magnetic nanospheres (Fig. 5e) or exposed to nanospheres containing magnetic nanoparticles at an iron concentration of 3.4 mM (Fig. 5f). Nuclear changes were abundant with nanospheres containing high levels of magnetic nanoparticles (16 mM iron, data not shown). These results suggest the

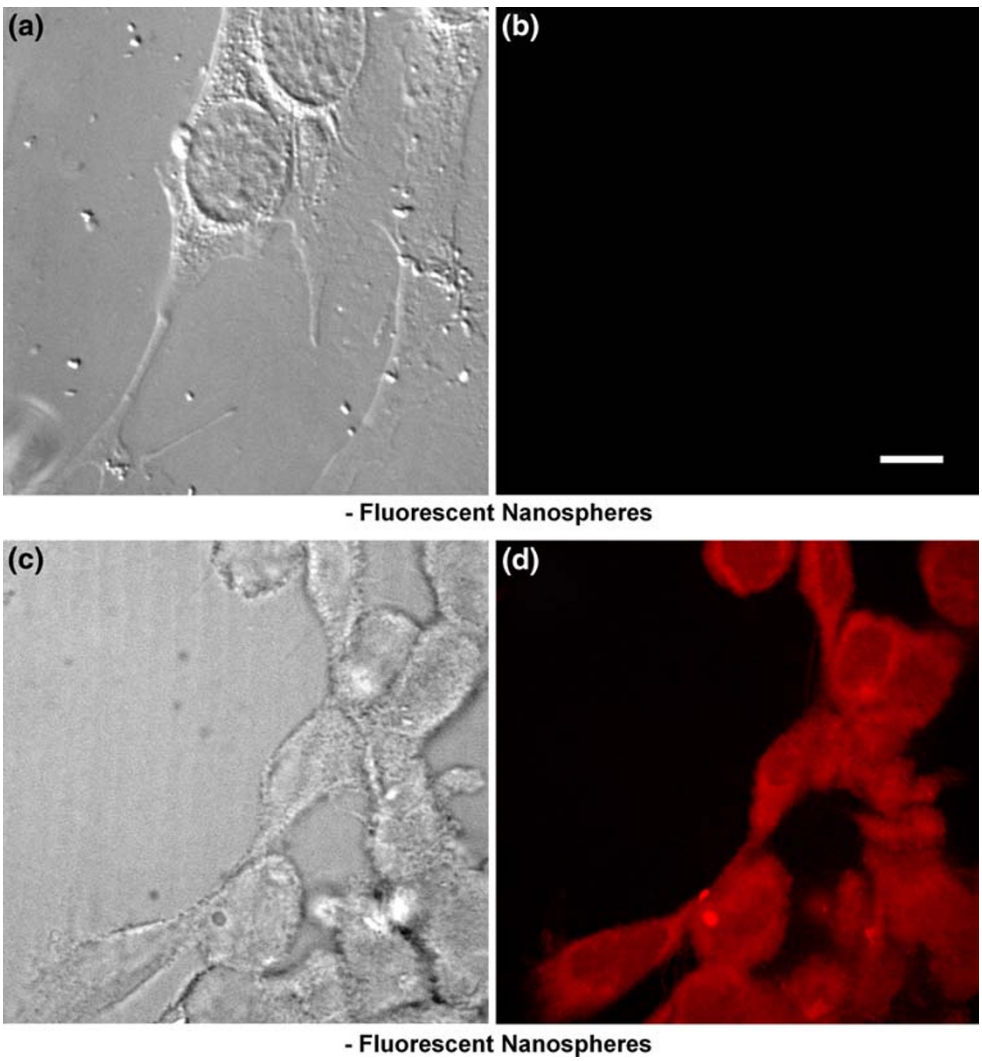

Fig. 4 Cellular uptake of magnetic nanospheres by PC12 cells. Representative (**a**) differential interference contrast (DIC) and corresponding (**b**) confocal images of PC12 cells not exposed to magnetic nanospheres. Representative (**c**) DIC and corresponding (**d**) confocal images of cells exposed to fluorescent magnetic nanospheres showing abundant internalization into cells. Scale bar in (**b**) = 10 μm and is valid for all images

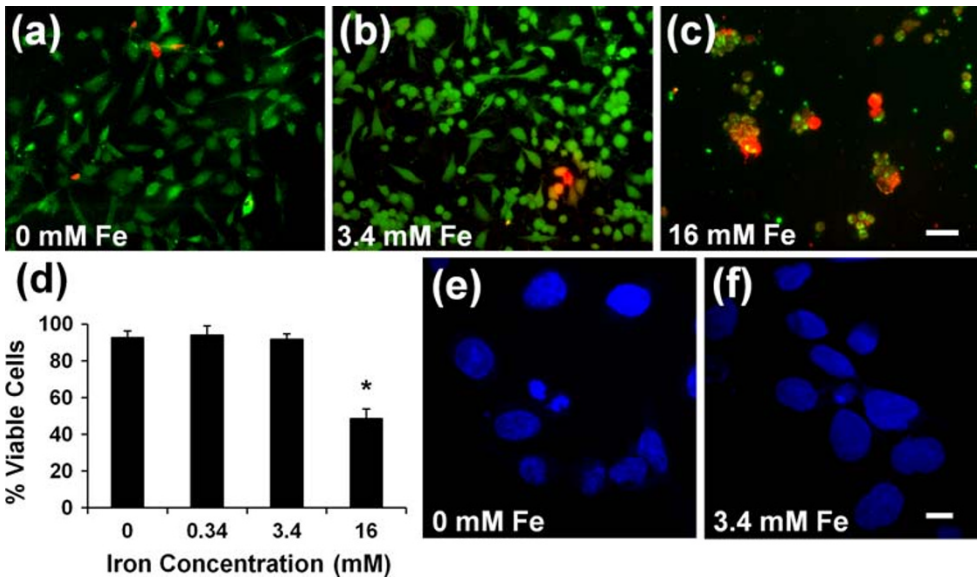

Fig. 5 Magnetic nanospheres have minimal cellular toxicity. Representative digital image of PC12 cells either not exposed (**a**), or exposed to magnetic nanospheres with iron concentrations of (**b**) 3.4 mM or (**c**) 16 mM for 48 h and double labeled with calcein AM (*green*) to show living cells and ethidium homodimer-1 (EthD1, red) to label dead or dying cells. Scale bar in (**c**) = 50 μm, and is valid for (**a**), (**b**) and (**c**). **d** Quantification revealed little cell toxicity up to 3.4 mM iron. Data are means ± standard deviations from three separate experiments, * $p = 0.001$ compared to cells not exposed to magnetic nanospheres (ANOVA and subsequent Tukey's post-hoc). Representative images show intact nuclei with little evidence of fragmentation, condensation or blebbing for cells (**e**) not exposed or (**f**) exposed to nanospheres containing 3.4 mM iron. Scale bar in (**f**) = 10 μm, and is valid for (**e**) and (**f**)

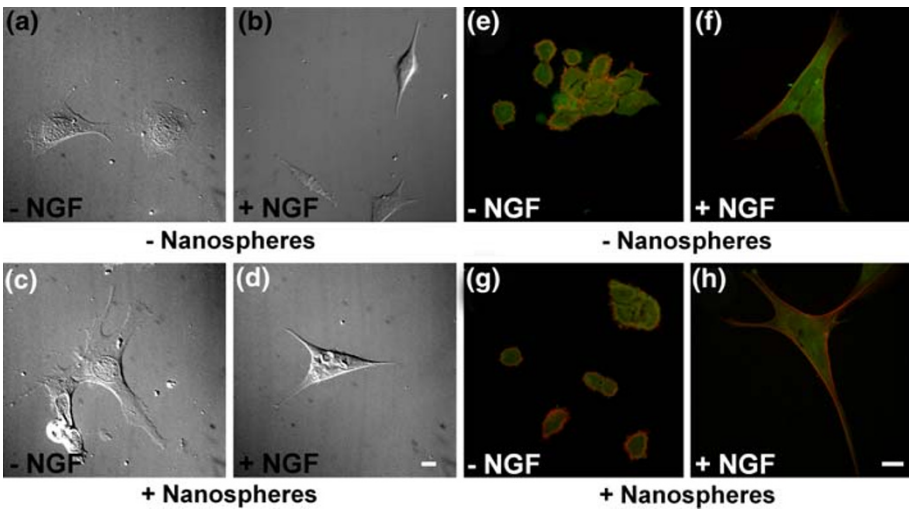

Fig. 6 Cells maintain normal morphology after exposure to magnetic nanospheres. Representative differential interference contrast (DIC) images of cells not exposed to magnetic nanospheres show typical morphology for PC12 cells (**a**) not treated or (**b**) treated daily with 100 ng/mL nerve growth factor (NGF) for 72 h. Normal morphology is maintained when cells are exposed to magnetic nanospheres and (**c**) not treated or (**d**) treated with NGF. Compared to cells not exposed to magnetic nanospheres and (**e**) not treated or (**f**) treated with NGF, cells exposed to magnetic nanospheres in the (**g**) absence or (**h**) presence of NGF have similar microtubule (*green*) and actin filament (*red*) cytoskeletal arrangements. Scale bar in (**d**) = 10 μm and is valid for (**a**) through (**d**). Scale bar in (**h**) = 10 μm and is valid for (**e**) through (**h**)

constructed nanosphere system assessed here had decreased cellular toxicity and induction of apoptosis compared to magnetic nanoparticles coated with PNIPAM or dimercaptosuccinic acid (DMSA) [14], or polyethylenoxide (PEO) triblock copolymers [33].

Magnetic Nanoparticles Minimally Affect Morphology and Neurite Outgrowth

Because central nervous system axons do not regenerate to an appreciable extent after damage [1], one application of

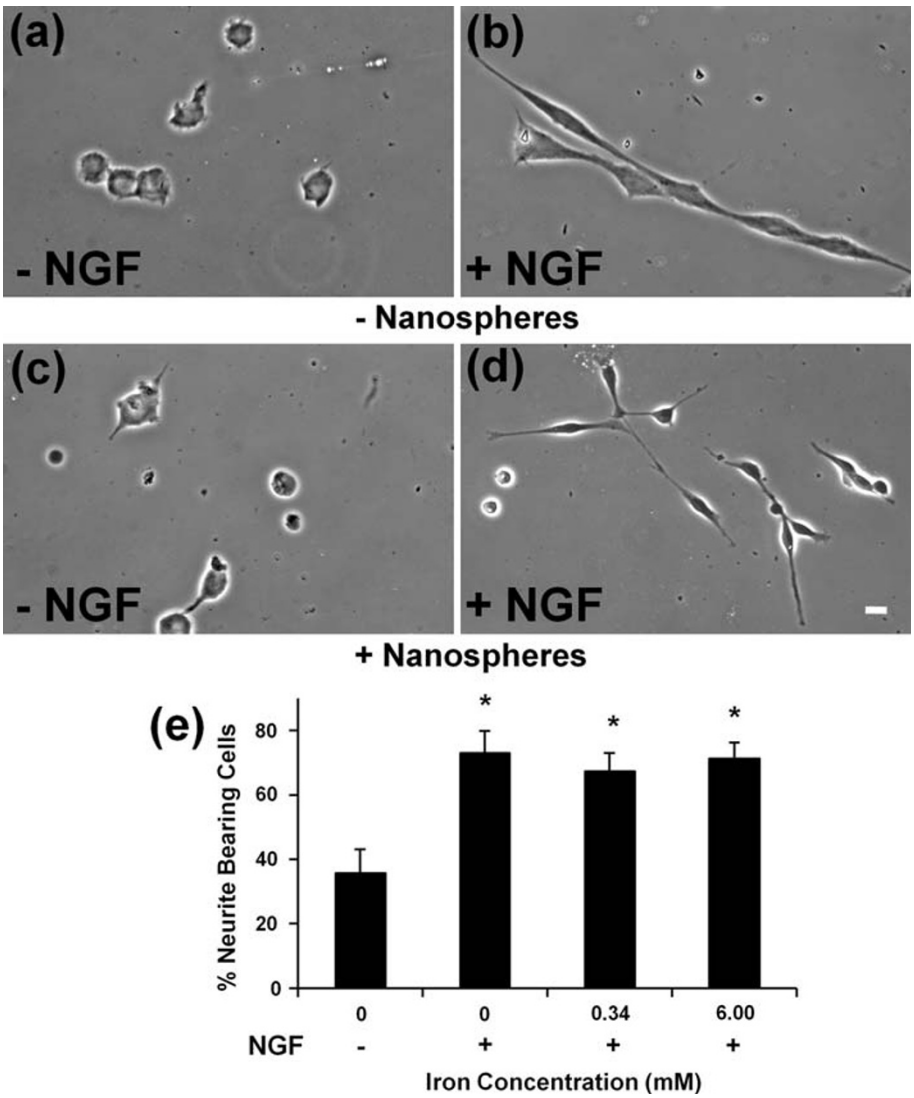

Fig. 7 Magnetic nanospheres do not inhibit neurite outgrowth. Compared to representative phase contrast images of PC12 cells not exposed to magnetic nanospheres and either (**a**) not treated or (**b**) treated daily with 100 ng/mL nerve growth factor (NGF), cells exposed to magnetic nanospheres with an iron concentration of 6.0 mM display similar morphology in the (**c**) absence or (**d**) presence of NGF. Scale bar in (**d**) = 10 μm, and is valid for (**a**) through (**d**). **e** Quantification of the percent of neurite bearing cells shows similar neurite outgrowth for cells either not exposed or exposed to magnetic nanospheres at iron concentrations of 0.34 and 6.0 mM and treated with NGF, all of which increased neurite outgrowth compared to cells not treated with NGF. Data in (**e**) are means ± standard deviations from three separate experiments, * $p = 0.001$ compared to cells not treated with NGF (ANOVA with subsequent Tukey post-hoc test)

the synthesized nanosphere system might be in the therapeutic manipulation of axon extension. If the nanospheres do not inhibit the extension of cellular processes, they hold promise for this application. We began to assess the potential use of the synthesized nanospheres for manipulating axon extension using PC12 cells, a neuronal model that extends neurites in response to exogenous addition of nerve growth factor (NGF). PC12 cells not exposed to magnetic nanospheres exhibited little formation of neurites in the absence of NGF, showing a spreading morphology with abundant lamellipodia (Fig. 6a). In contrast, cells exposed to NGF displayed a neuron-like morphology with 1–2 neurites/cell (Fig. 6b). Exposure to magnetic nanospheres containing nanoparticles at 3.4 mM iron did not alter cell morphology in the absence (Fig. 6c) or presence (Fig. 6d) of NGF. Because neuron structure is determined by the arrangement of cytoskeletal microtubules and actin filaments, we next assessed the effect of magnetic nanospheres on PC12 cytoskeleton. For cells not exposed to magnetic nanospheres, typical arrangements of cytoskeletal elements were observed. Here, tubulin was abundant in the central regions of cells, and actin filaments were mainly localized to the cell cortex for rounder cells observed in the absence of NGF (Fig. 6e) and for cells extending neurites in the presence of NGF (Fig. 6f). Cytoskeletal arrangements were similar for cells exposed to magnetic nanospheres (3.4 mM iron) in both the absence (Fig. 6g) and presence (Fig. 6h) of NGF. However, it may be possible that actin filament concentration was slightly increased in cells exposed to magnetic nanospheres (compare Fig. 6 (e, f) with Fig. 6 (g, h)). These results stand in contrast to the decreased actin filament content seen with DMSA coated magnetic nanoparticles [14]. Thus, it appears that the constructed nanosphere system has no detrimental effects on cell morphology and cytoskeleton, and may enhance the formation of actin filaments.

The few effects on cell morphology indicate promise for the synthesized system for manipulating axon

regeneration. However, if the nanospheres adversely affect neurite outgrowth, their therapeutic potential is decreased. Qualitative assessment from phase-contrast images of cells not exposed to magnetic nanospheres showed little neurite outgrowth in the absence of NGF (Fig. 7a), whereas daily treatment with 100 ng/mL NGF led to cells that readily extended neurites and exhibited the formation of cellular contacts (Fig. 7b). Similar levels of neurite extension were seen in cells exposed to nanospheres containing magnetic nanoparticles with an iron concentration of 6.0 mM for 48 h prior to 72 h without (Fig. 7c) or with 100 ng/mL NGF (Fig. 7d). In the latter, cells also formed cell to cell contacts. These results indicated that exposure to non-toxic levels of magnetic nanospheres did not inhibit the elaboration of neurites. An exciting application of this system is its implementation to enhance axon growth and manipulate axon trajectories in combination with endogenous responses to magnetic fields [2–4]. We are currently assessing baseline and magnetic field-induced responses of several neuronal models to the nanospheres.

Conclusions

In summary, we report the synthesis, actuation and dose-dependent modulation of a multifunctional nano-scale system consisting of all FDA-approved bio-polymers. Based on these results, we conclude that the designed nanomagnets possess dual capability of regulating temperature and tuning size, i.e., the mesh density by remote controlled actuation. These special features carry the potential for synergistic application of heat and sustained release of small molecules in therapeutics. Moreover, compared to currently available systems, cytotoxicity is remarkably reduced by the stealth polymer encapsulation around the magnetic core and allowing higher intracellular concentrations of magnetic nanoparticles. One exciting application for this system may be using either unaltered or derivatized nanospheres in conjunction with magnetic fields to manipulate axon growth. The neurite growth pattern seen at high nanosphere concentrations is especially promising for further studies with effect on primary neurons in terms of axon regeneration following nervous system injury.

Acknowledgments Supported by the TWU Department of Biology, the SEMO Physics and Engineering Physics Department, and grants from the TWU Research Enhancement and Summer Stipend programs (to DLH), the Texas Higher Education Coordinating Board Closing the Gaps program (to DLH), and the SEMO Grants and Research Funding Committee (to SG). We sincerely appreciate Dr. Zhibing Hu's generosity for laboratory access.

References

1. R.L. Ruff, L. McKerracher, M.E. Selzer, Ann. NY. Acad. Sci. **1142**, 1–20 (2008)
2. M.Y. Macias, J.H. Battocletti, F.A. Pintar, D.J. Maiman, Bioelectromagnetics **21**, 272–286 (2000)
3. C.D. McCaig, A.M. Rajnicek, B. Song, M. Zhao, Physiol. Rev. **85**, 943–978 (2006)
4. S. Kim, W.S. Im, L. Kang, S.T. Lee, K. Chu, B.I. Kim, J. Neurosci. Meth. **174**, 91–96 (2008)
5. D.A. La Van, T. McGuire, R. Langer, Nat. Biotechnol. **21**, 1184–1191 (2003)
6. C.M. Niemeyer, Angew. Chem. Int. Ed. Engl. **40**, 4128–4158 (2001)
7. A.P. Alivisatos, Nat. Biotechnol. **22**, 47–52 (2004)
8. A.J. DeMello, Nature **442**, 394–402 (2006)
9. J. Lutz, S. Stiller, A. Hoth, L. Kuafner, R. Cartier, Biomacromolecules **7**, 3132–3138 (2006)
10. A. Peppas, J. Hilt, A. Khademhosseini, R. Langer, Adv. Mater. **18**, 1345–1360 (2006)
11. R. Bashir, Adv. Drug. Deliver. Rev. **56**, 1565–1586 (2004)
12. T. Liu, S. Hu, K. Liu, D. Liu, S. Chen, J. Magn. Magn. Mater. **304**, e397 (2006)
13. D.C. Harsh, S.H. Gehrke, J. Controlled Release **17**, 175 (1991)
14. T.R. Pisanic II, J.D. Blacwell, V.I. Shubayev, R.R. Finones, S. Jin, Biomaterials **28**, 2572–2581 (2007)
15. F. Mohamed, P. Marchettini, O.A. Stuart, M. Urano, P.H. Sugarbaker, Ann. Surg. Oncol. **10**, 463–468 (2003)
16. Z.B. Hu, Y. Chen, C. Wang, Y. Zheng, Y. Li, Nature **393**, 149–152 (1998)
17. T. Cai, M. Marquez, Z. Hu, Langmuir **23**, 8663–8666 (2007)
18. J. Lutz, A. Hoth, Macromolecules **39**, 893–896 (2006)
19. S. Ghosh, C. Yang, T. Cai, Z. Hu, A. Neogi, J. Phys. D Appl. Phys. **42**(13), 135501 (2009) (8 pp)
20. D.T. Eddington, D.J. Beebe, J. Microelectromech. S. **103**, 586–593 (2004)
21. Q. Yu, J.M. Bauer, J.S. Moore, D.J. Beebe, Appl. Phys. Lett. **78**, 2589–2591 (2001)
22. S.R. Sershen, G.A. Mensing, N.J. Halas, D.J. Beebe, J.L. West, Adv. Mater **17**, 1366–1368 (2005)
23. N.K. Prasad, K. Rathinasamy, D. Panda, D. Bahadur, J. Mater. Chem. **17**, 5042–5051 (2007)
24. M. Ma, Y. Wu, J. Zhou, Y. Sun, Y. Zhang, N. Gu, J. Magn. Magn. Mater. **268**, 33–39 (2004)
25. B. Garner, T. Cai, S. Ghosh, Z. Hu, A. Neogi, Appl. Phys. Exp. **2**, 057001–057003 (2009)
26. F. Bertorelle, C. Wilhelm, J. Roger, F. Gazeau, C. Ménager, V. Cabuil, Langmuir **22**, 5385–5391 (2006)
27. L. Hasadsri, J. Kreuter, H. Hattori, T. Iwasaki, J.M. George, J. Biol. Chem. **284**, 6972–6981 (2009)
28. C. Yu, J. Zhao, Y. Guo, C. Lu, X. Ma, Z. Gu, J. Biomed. Mater. Res. **87A**, 364–372 (2008)
29. S.A. Townsend, G.D. Evrony, F.X. Gu, M.P. Schulz, R.H. Brown Jr, R. Langer, Biomaterials **28**, 5176–5184 (2007)
30. D. Demirgöz, A. Garg, E. Kokkoli, Langmuir **24**, 13518–13524 (2008)
31. L. Yang, H. Mao, Y.A. Wang, Z. Cao, X. Peng, X. Wang, H. Duan, C. Ni, Q. Yuan, G. Adams, M.Q. Smith, W.C. Wood, X. Gao, S. Nie, Small **5**, 235–243 (2009)
32. Y. Cho, R. Shi, A. Ivanisevic, R.B. Borgens, Nanotechnol. **20**, 2757102U (2009)
33. O. Häfeli, J.S. Riffle, L. Harris-Shekhawat, A. Carmichael-Baranauskas, F. Mark, J.P. Dailey, D. Bardenstein, Mol. Pharm. (2009). doi: 10.1021/mp900083m